Ji, Y., Yoon, J. S., Zang, A., Wu, W. (2021): Mitigation of injection-induced seismicity on undrained faults in granite using cyclic fluid injection: A laboratory study. - International Journal of Rock Mechanics and Mining Sciences, 146, 104881.

https://doi.org/10.1016/j.ijrmms.2021.104881

Mitigation of Injection-induced Seismicity on Undrained Faults in Granite using Cyclic Fluid Injection: A Laboratory Study

Yinlin Ji [a, d], Jeoung Seok Yoon [b], Arno Zang [c], Wei Wu [a, *]

[a] School of Civil and Environmental Engineering, Nanyang Technological University, 639798, Singapore.

[b] DynaFrax UG, Helmholtzstrasse 6, 14467 Potsdam, Germany.

[c] Helmholtz Centre Potsdam GFZ German Research Centre for Geosciences, Telegrafenberg, 14473 Potsdam, Germany.

[d] Present Address: Helmholtz Centre Potsdam GFZ German Research Centre for Geosciences, Telegrafenberg, 14473 Potsdam, Germany.

[*] Corresponding author: Wei Wu (wu.wei@ntu.edu.sg)

Abstract

Cyclic fluid injection has been demonstrated as a plausibly effective and controllable strategy to mitigate the seismic risks during hydraulic stimulation. The mechanism involved remains largely unconstrained, and our ability to control the activation of critically stressed, locally undrained faults is still limited. Injection-induced activation of these faults can be one of the most threatening scenarios as they likely perturb the stability of nearby faults beyond the stimulation volume. Here, we perform a series of laboratory fluid injection tests on critically stressed, locally undrained faults in low-permeability granite to offer insights into cyclic fluid injection as a possible solution for seismic risk mitigation. Our results show that cyclic fluid injection promotes fluid pressure diffusion on the faults, but a reduction in seismic moment release depends on several cycle-related factors, such as the critical injection pressure and injection frequency. Particularly, cyclic fluid injection could be inefficient for fluid pressure diffusion if the critical injection pressure is very close to the predicted pressure at fault failure, or over-reduced to cause excess fluid injection and long-term frictional healing. A proper design of injection parameters is thus essential to balance the energy budget between the seismic energy and hydraulic energy. Our study reveals that the effectiveness of cyclic fluid injection is also dependent on fault drainage conditions, stimulation requirements, as well as dynamic responses of faulted reservoirs, which could guide the future development of cyclic fluid injection.

Keywords: Cyclic fluid injection; Injection-induced seismicity; Undrained laboratory fault; Seismic risk mitigation.

1 Introduction

In unconventional energy extraction (e.g., geothermal or shale oil and gas operations), fluid injection into faulted reservoirs has been linked to a dramatic rise in seismicity rate.[1-3] The injection-induced fluid pressurization could either weaken fully drained faults through a uniform reduction in effective normal stress or destabilize locally undrained faults with lower permeability than drained faults through dynamic rupture extending beyond the reservoirs. The shear slip of natural and hydraulically induced faults within the reservoirs is expected to increase the possibility of fault permeability enhancement.[4-6] However, the uncontrollable release of tectonic energy from a runaway rupture is believed as the main cause of destructive earthquakes,[7-9] which has become a major barrier to the development of unconventional energy.

Several attempts have been made to mitigate the seismic risks associated with fluid injection, such as the traffic light system[10] and borehole seismometer network.[11] Cyclic fluid injection has been used as a common approach for improving oil and gas recovery[12-14] and also considered as an effective and controllable strategy to manage anthropogenic earthquakes based on the concept of fatigue hydraulic fracturing.[15,16] At Äspö Hard Rock Laboratory in Sweden, the maximum magnitude (M_w) and breakdown pressure from cyclic fluid injection were lower than those from monotonic fluid injection.[17,18] Particularly, the full waveform analysis showed that the *b*-value in cyclic fluid injection was higher than that in the monotonic fluid injection,[19] indicating that cyclic fluid injection modified the frequency-magnitude distribution towards a safer stimulation treatment with smaller and lesser large magnitude seismic events. The cyclic fluid injection at Pohang geothermal project in Korea successfully limited the maximum magnitude below a target threshold of M_w 2.0 in August 2017,[20,21] but a damaging earthquake of M_w 5.5 unexpectedly occurred in Decemeber 2017.[22] Numerical studies have shown that the spatio-temporal distribution of seismic events can be adjusted by cyclic fluid injection.[23,24] Nevertheless, the current field experiments with pre-determined injection parameters may not accommodate the dynamic evolution of the reservoirs during fluid injection. To further improve the effectiveness of cyclic fluid injection, it is critical to examine the cycle-related factors that dictate the reservoir response and especially fault activation.

Laboratory fluid injection tests have advantages to simulate the in-situ stress and fluid injection conditions and isolate the cycle-related factors from complex geologic environments. Previous test results indicate that the dynamic slip of uniformly pressurized faults occurs when the fluid pressure at fault failure reaches that predicted by the Mohr-Coulomb failure criterion, but the fluid pressure at fault failure can overshoot the predicted pressure on non-uniformly pressurized faults.[25-27] The fluid overpressure on locally undrained faults may cause the slip area exceeding the pressurized area, resulting in fault slip propagating in the unpressurized area.[28,29] Cyclic fluid injection into simulated faults in permeable sandstone samples promotes the transition from the stable to unstable slip,[30] while cyclic fluid injection into natural faults in low-permeability granite samples demonstrates a reduction in slip rate at fault failure.[31] These results suggest that the drainage conditions of the faults and adjacent rocks strongly influence the occurrence of seismic events. Particularly, the injection-induced slip of locally undrained faults likely leads to felt earthquakes, but their response to cyclic fluid injection remains poorly understood. Additionally, pressure-controlled fluid injection is commonly adopted as it is readily controlled in the laboratory.[5,26,27,32] However, volume-controlled fluid injection is realistically operated in the field,[11,17,21] which should be carefully managed in the laboratory to avoid a drastic increase in fluid pressure and the resultant sample jacket breakage and confining oil leakage.

We conducted fluid injection tests on locally undrained faults using pressure-controlled and volume-controlled fluid injection to provide insights into cyclic fluid injection as a plausible solution for seismic risk mitigation. We then compared the seismic moment, seismic energy, and hydraulic energy of the monotonic and cyclic injection tests as well as previous field injection experiments to highlight the effectiveness of cyclic fluid injection. We finally discussed the possible development of cyclic fluid injection in seismic risk mitigation.

2 Materials and Methods

A series of fluid injection tests were carried out on sawcut faults in Bukit Timah granite. The granite is sourced from central Singapore and composed of 62% feldspar, 32% quartz, 5% biotite, and 1% hornblende. The bulk density, water content, and porosity are 2660 kg/m^3, 0.07%, and 0.26%, respectively. The uniaxial compressive strength, Young's modulus, and intrinsic permeability are 238 MPa, 73.8 GPa, and 1.3 μD, respectively.[33]

We selected a granite sample from a 50-mm-diameter cylindrical core without visible cracks on the surfaces and ground the sample with flat and parallel ends to 100 mm long. We used a diamond saw to cut the sample at 30° to the core axis and polished the sawcut surfaces using sandpaper with 25.6 μm particle size. We then drilled two boreholes with a 2 mm diameter to facilitate distilled water flowing from the coreholders to the fault. We finally fixed the sample on the coreholders and isolated it from the confining oil using two layers of Teflon jackets.

We used the MTS 815 rock mechanics test system to conduct the fluid injection tests (Fig. 1a). We injected the fluid through the lower borehole, and both fluid pressures in the lower (injection) and upper (monitoring) boreholes were measured by the dual hydraulic pumps (Vindum Model VP-12K). The effective normal (σ'_n) and shear (τ) stresses on the fault were servo-controlled by the axial stress (σ_1) and confining pressure (σ_3) and determined as

$$\sigma_n' = (\sigma_3\text{-p}) + (\sigma_1\text{-}\sigma_3)\cos^2\psi \tag{1}$$

$$\tau = (\sigma_1\text{-}\sigma_3)\sin\psi\cos\psi \tag{2}$$

where Ψ is the fault inclination angle to the core axis; and p is the fluid pressure on the fault.

The load point displacement (Δl) was recorded by a linear variable differential transformer (LVDT) installed inside the axial piston. The shear displacement along the fault (dl_s) was obtained by excluding the contributions from the elastic deformation of the test system and rock blocks

$$dl_s = \frac{\Delta l - \frac{\Delta F}{K_b} - \frac{\Delta F}{K_m}}{\cos\psi} \tag{3}$$

where ΔF is the axial force; K_b is the elastic stiffness of the rock blocks (1447 kN/mm); K_m is the elastic stiffness of the test system (667 kN/mm).[34] The stress and displacement were measured at a sampling frequency of 100 Hz, and the fluid pressures were recorded at a sampling frequency of 1 Hz.

We performed 13 monotonic and cyclic fluid injection tests with pressure-controlled and volume-controlled conditions, respectively, under 11 and 21 MPa normal stresses (Table 1). As shown in Fig. 1b, we first applied a normal stress, degassed the pore system, and saturated the sawcut fault with 1 MPa fluid pressure. Here we assume that the pore system is fully saturated, and fluid is incompressible. Second, we increased the load point displacement at a constant rate of 1 μm/s until the fault failed and obtained the maximum shear stress as the shear strength. Third, we maintained the shear stress at 80% of the shear strength and assumed the fault approaching a critical stress state. We subsequently injected the fluid through the injection borehole until the fault activation occurs again. The four fluid injection strategies were carried out in different fluid injection tests. For the pressure-controlled monotonic injection tests, the fluid was injected at a pressure rate of 0.01 MPa/s (Fig. 2a). The pressure-controlled cyclic injection tests were conducted at the same pressure rate by changing the fluid pressure between the initial injection pressure (1 MPa) and critical injection pressure (Fig. 2b), which was defined as 95% of the injection pressure at fault failure obtained in the pressure-controlled monotonic injection test. In the volume-controlled monotonic injection tests, the fluid was injected at a volume rate of 0.2 mL/min (Fig. 2c). The injection rate in the volume-controlled cyclic injection tests alternated between 0.2 and 0 mL/min, and each cycle was terminated when the critical injection pressure (i.e., 95%, 90%, and 85% of the injection pressure at fault failure obtained in the volume-controlled monotonic injection test) was achieved (Fig. 2d). The duration of injection suspension (0 mL/min) between the adjacent cycles was 300 s.

3 Results and discussion

3.1 Laboratory observations

The fluid injection test results show that the failure of the fault is accompanied by a sudden shear stress drop and an abrupt shear displacement jump (Figs. 3 and 4), which is known as a dynamic slip.[35] The occurrence of dynamic slip is due to the slip weakening rate of the fault is higher than the elastic unloading rate of the test system.[36] After that, when the shear displacement further increases, the shear stress recovers to the initial value due to the re-formation and re-strengthening of asperity contacts.[37,38]

For the pressure-controlled monotonic injection test under 11 MPa normal stress, a fault slip occurs when the injection pressure rises to 3.68 MPa, while the monitoring pressure at fault failure remains lower at 1.03 MPa (Fig. 3a). The critical injection pressure in the pressure-controlled cyclic injection test is set as 3.50 MPa (i.e., 95% of 3.68 MPa). During the first cycle, the injection pressure increases to the critical injection pressure and subsequently decreases to the initial injection pressure. The fault slip occurs when the injection pressure reduces to 3.36 MPa (Fig. 3b) owing to stress relaxation on the fault.[16] The monitoring pressure at fault failure remains very low (1.05 MPa). The difference between the injection and monitoring pressures at fault failure reveals that the failure of the fault can be attributed to the injection-induced local slip, which is initiated in the pressurized area and accompanied by micro-seismic events.[30,39,40] We attribute the occurrence of fault slip during the first cycle to the high critical injection pressure. To better observe the fault response to pressure-controlled cyclic injection, we perform another pressure-controlled cyclic injection test with a critical injection pressure of 3.33 MPa (i.e., 90% of 3.68

MPa). The results show that no slip occurs until the monitoring pressure reaches 3 MPa in the 33rd cycle (Fig. 3c), which is the fluid pressure at fault failure predicted by the Mohr-Coulomb failure criterion. This is mostly due to the enhanced shear strength caused by frictional healing after a long-term fluid injection. The shear displacement slightly increases with fluctuations, indicating stable fault creep occurring with cyclic injection and associated with poroelastic coupling of stress and fluid pressure on the fault.[32] When the normal stress is 21 MPa and the critical injection pressure is 13.94 MPa (i.e., 95% of 14.67 MPa), the fault also fails during the first cycle in the pressure-controlled cyclic injection test, and the difference between the injection and monitoring pressures becomes larger than that under 11 MPa normal stress (Table 1). Our results indicate that cyclic fluid injection could be inefficient to promote fluid pressure diffusion on the fault if the critical injection pressure is very close to the predicted pressure at fault failure.

Similarly, as shown in Fig. 4a, the volume-controlled monotonic injection test under 11 MPa normal stress is used to estimate the injection pressure at fault failure (3.72 MPa), and the corresponding volume-controlled cyclic injection tests are conducted with three critical injection pressures (3.53, 3.38 and 3.16 MPa, as 95%, 90% and 85% of 3.72 MPa, respectively). When the critical injection pressures are 3.53 and 3.38 MPa, the fault instability occurs during the first cycle, and the monitoring pressures at fault failure are still around 1 MPa. However, when the critical injection pressure further decreases to 3.16 MPa, the fault is activated during the 27th injection cycle (Fig. 4b). Importantly, the monitoring pressure at fault failure almost reaches the injection pressure, indicating that cyclic fluid injection significantly promotes the uniform distribution of fluid pressure on the fault. This test also shows a profound stable fault creep before the occurrence of a dynamic slip. For all the cyclic fluid injection tests under 21 MPa normal stress, the fault fails during the first cycle, because the fluid is largely constrained in the highly squeezed fault. The further decrease in the critical injection pressure may enhance the effectiveness of cyclic fluid injection, but the critical injection pressure should be larger than the fluid pressure at fault failure predicted by the Mohr-Coulomb failure criterion as a critical injection pressure lower than this predicted value cannot lead to fault failure.[25]

3.2 Fluid pressure heterogeneity during cyclic fluid injection

Our results show that the injection and monitoring pressures vary at different growth rates during cyclic fluid injection, depending on the normal stress and critical injection pressure. The transition from locally undrained to fully drained condition of the fault is accompanied by reducing asperity mechanical interaction on the fault and advancing pressure spike formation between sheared asperities. The reduced asperity mechanical interaction associated with lesser and weaker asperity contacts is presumably due to a more uniform reduction in effective normal stress during the transition from locally undrained to fully drained condition.[41-43] We thus use the degree of fluid pressure heterogeneity (D_f) to quantify fluid pressure distribution on the fault, which is defined as the ratio of the difference between the injection (P_{inj}) and monitoring (P_{mon}) pressures to the injection pressure:[25]

$$D_f = \frac{P_{inj} - P_{mon}}{P_{inj}} \tag{4}$$

Lower degree of fluid pressure heterogeneity signifies a more homogenous fluid pressure distribution on the fault. Fig. 5 presents the degree of fluid pressure heterogeneity as a function of the critical injection pressure ratio, defined as the ratio of the critical injection pressure to injection pressure at fault failure, under 11 MPa and 21 MPa normal stresses. The ratio is considered as 100% in the pressure-controlled and volume-controlled monotonic injection tests. For the pressure-controlled cyclic injection tests under both the normal stresses, the degree of fluid pressure heterogeneity slightly decreases. The volume-controlled cyclic injection tests remarkably reduce the degree of fluid pressure heterogeneity under 11 MPa normal stress, and the reduction is promoted when the critical injection pressure further drops from the injection pressure at fault failure. However, the degree of fluid pressure heterogeneity remains close to 1 under 21 MPa normal stress, suggesting that cyclic fluid injection is less effective in promoting fluid pressure migration on the fault under higher normal stress. Lower critical injection pressure and lower injection frequency are expected under higher normal stress to promote a uniform fluid pressure distribution on the fault.

3.3 Seismic moment release due to cyclic fluid injection

The injection-induced seismic moment can be predicted using injected volume.[8,44,45] Although the prediction accuracy is affected by several assumptions (such as fluid injection near mapped faults and uniform fluid pressure distribution on the faults), these models have been validated for self-arrested events. The model proposed by McGarr[44] is used to estimate the maximum seismic moment as

$$M_0(\max) = G\Delta V \tag{5}$$

where G and ΔV are the modulus of rigidity for reservoir rocks and injected volume, respectively. In our study, G represents the combined rigidity of the test system and the fault (4.2 GPa) according to the method proposed by Ji et al.[33]

The model from Galis et al.[8] can predict the maximum arrested moment as

$$M_0(\max - arr) = \gamma \Delta V^{3/2} \tag{6}$$

where γ is the reservoir parameter and defined as

$$\gamma = \frac{0.4255}{\sqrt{\Delta\tau}}\left(\frac{\kappa\mu_{\mathrm{d}}}{h}\right)^{3/2} \tag{7}$$

where κ is the bulk modulus of reservoir rocks and estimated as 2/3 of the combined rigidity (2.8 GPa);[46] h is the reservoir thickness and assessed as the ratio of the sample volume to fault area (0.05 m);[8] $\Delta\tau$ and μ_d are the shear stress drop and dynamic friction coefficient, respectively (Table 1). Here the shear stress drop is the difference between the critical and minimum shear stresses during fault slip, and the dynamic friction coefficient is the ratio of the minimum shear stress during a dynamic slip to effective normal stress.[47] As the effective normal stress is non-uniform on the fault, we estimate the mean fluid pressure over the fault by averaging the injection and monitoring pressures at fault failure, which approaches that predicted by the Mohr-Coulomb failure criterion[48], and then obtain the effective normal stress by subtracting the mean fluid pressure from the applied normal stress. In this study, γ is calculated as 2.0×10^{12}.

The seismic moment release of the injection-induced fault slip is almost purely seismic (Figs. 3 and 4) and thus determined based on the definition of seismic moment[49]

$$M_0 = GAd \tag{8}$$

where A is the fault area (3.9×10^{-3} m^2), and d is the slip displacement (Table 1). Because the length of the sawcut fault (centimeter scale) is far smaller than the critical nucleation length of a granite fault (meter scale),[50] the laboratory-scale sample cannot fully accommodate a fault rupture.

Fig. 6 shows the seismic moment release of injection-induced slip in our tests. The upper bounds of the models suggested by McGarr[44] and Galis et al.[8] are constructed with the combined rigidity of the test system and the fault (4.2 GPa) and laboratory-scale reservoir parameter (2.0×10^{12}), respectively. The seismic moment release is calculated using Eq. (8) with the same combined rigidity. All of our data points are below the upper bounds, and the seismic moment release increases linearly with larger injected volume under each normal stress. The injected volume and seismic moment release in the cyclic injection tests are lower than those in the monotonic injection tests under both pressure-controlled and volume-controlled conditions. In the pressure-controlled cyclic injection tests, fluid depressurization results in the largest reduction in seismic moment release, which could be achieved by decreasing cumulative fluid volume to reduce the seismic risks in the field.[51] Although lowering the critical injection pressure reduces the degree of fluid pressure heterogeneity (Fig. 5), the seismic moment release in the cyclic injection test with 85% of the injection pressure at fault failure (aCV3) is surprisingly comparable to that in the monotonic injection test (aMV) with the same normal stress and injection rate. This is presumably because the long-term injection process with a relatively slow and uniform increase in fluid pressure over the fault promotes restrengthening of asperity contacts.[52] The cyclic injection test with 90% of the injection pressure at fault failure (aCP2) also shows frictional healing accompanied by a flattening fluctuation in shear displacement caused by the long-term fluid injection (Fig. 3c).

3.4 Energy budget in cyclic fluid injection

The energy budget of injection-induced seismicity can be assessed using the relationship between seismic energy and hydraulic energy to anticipate the seismic energy release due to fluid injection.[15,53-55] Here we consider the seismic energy mainly from the dynamic slip characterized by a shear stress drop and a shear displacement jump (Figs. 3 and 4). The seismic energy (E_r) released from a seismic event can be calculated based on an empirical relationship,[56,57]

$$\log(\mathrm{E_r}) = 1.5M_w + 4.8 \tag{9}$$

where M_w is the moment magnitude and estimated as,[58]

$$M_w = \frac{\log M_0}{1.5} - 6.07 \tag{10}$$

In the field, both the seismic and aseismic motions can occur. However, in our tests, a sudden increase in shear displacement is accompanied by an abrupt drop of shear stress, and the aseismic motion cannot be clearly detected using the current test setup. This limitation suggests that the seismic energy estimated in our case is thus underestimated and serve as a lower boundary.

Given the assumptions that the seismic events resulted from the hydro-shearing process and the energy consumption by the hydro-fracturing process is neglected, the hydraulic energy (E_h) is determined as,[56]

$$E_h = \int_{t_1}^{t_2} P\,q\,dt \tag{11}$$

where P and q are the injection pressure and injection rate at time t, respectively.

Fig. 7a summarizes the relationship between the seismic energy and hydraulic energy in various experimental, numerical, and field cases. The seismic energy shows a tendency to increase with larger hydraulic energy. The ratio of the seismic energy to hydraulic energy is plotted and known as the seismic injection efficiency.[59] The field injection experiments in Äspö Hard Rock Laboratory and the corresponding numerical simulations are also included and show that the evolution of seismic energy can be directly correlated to the change in hydraulic energy during cyclic fluid injection.[15,17,18] For our tests, the seismic injection efficiency ranges from 1.3×10^{-5}% to 1.3×10^{-1}%, which is similar to the typical ranges of the field cases associated with fault activation (1.0×10^{-5}% – 1.0×10^{-1}%).[59] The zoomed-in view highlights that the seismic energy from our cyclic injection tests is lower than that from the monotonic injection tests (Fig. 7b), which is consistent with the numerical and field observations. The hydraulic energy from the cyclic injection tests is also smaller than that from the monotonic injection tests, in contrast to the numerical and field cases. In the field injection experiments, the excessive hydraulic energy is attributed to fluid leak-off into adjacent fracture networks. However, fluid pressure diffusion occurs primarily along the fault in our tests, and no obvious fractures are observed in the granite matrix after the tests.

3.5 Implications for seismic risk mitigation using cyclic fluid injection

Our study demonstrates that cyclic fluid injection controls the seismic energy and hydraulic energy from locally undrained faults in low-permeability rocks, but the injection strategy should be tailored to specific fault settings. For fully drained faults in high-permeability rocks, cyclic fluid injection promotes the occurrence of unstable slip due to the increase in critical fault stiffness, but the reduction in critical injection pressure restricts the unstable slip.[30] Both locally undrained and fully drained faults are possibly encountered in faulted reservoirs, so different fault responses challenge us to mitigate the seismic risks from complex fault systems. Additionally, both the hydro-fracturing and hydro-shearing processes are involved in the field experiments[60] and can be determined from the focal mechanisms,[61] but play different roles in the occurrence of seismic events. Laboratory fluid injection tests demonstrate that the hydro-fracturing process dominates the injection-induced failure of intact rocks and releases the seismic energy to create fracture networks, and cyclic fluid injection reduces the maximum acoustic emission amplitude.[62,63] In our tests, when the hydro-shearing process governs the injection-induced failure of faulted rocks, cyclic fluid injection promotes fluid pressure diffusion and reduces seismic energy release. Hence, cyclic fluid injection could be effective to mitigate the seismic risks from both the hydro-fracturing and hydro-shearing processes.

In the field, cyclic fluid injection can be further developed to modulate the hydro-fracturing and hydro-shearing processes in different hydraulic stimulation stages, depending on operational requirements (e.g., promoting generation of fracture networks) and monitoring feedbacks (e.g., reducing possibility of earthquake occurrence). Cyclic fluid injection with higher critical injection pressure (i.e., closer to breakdown pressure) and higher injection frequency (i.e., shorter cycle duration) could predominately improve the effectiveness of hydraulic fracturing.[20] After that, both critical injection pressure and injection frequency could be reduced to mainly enhance the permeability of natural and hydraulically induced faults. Meanwhile, dominating large faults under either locally undrained or fully drained conditions should be considered in determining the critical injection pressure. Particularly, if the maximum magnitude approaches a target threshold, the critical injection pressure and injection frequency must be carefully tailored to mitigate the seismic risks.[17,21] In future, we may see the joint discussion of asperity interaction and failure along faults (mechanical instability) and the analogue of high-pressure patches hydraulically communicating along faults (hydraulic instability) beneficial.

4 Conclusions

We carried out fluid injection tests on critically stressed, locally undrained faults in low-permeability granite to provide insights into cyclic fluid injection as a potential solution for seismic risk mitigation. Our results show that cyclic fluid injection promotes fluid pressure diffusion on the faults and reduces the degree of fluid pressure heterogeneity. The critical injection pressure is vital to the effectiveness of cyclic fluid injection and should be larger than the predicted pressure at fault failure. If the critical injection pressure is over-reduced, the seismic moment release may not decrease significantly due to excess fluid injection and long-term frictional healing. The hydraulic energy in our cyclic injection tests on locally undrained faults is lower than that in the monotonic injection tests. This is in contrast with the observations in previous numerical and field cases possibly containing both locally undrained and fully drained faults.

Our data indicate that determining a proper critical injection pressure is essential to improve the performance of cyclic fluid injection. However, it is challenging to achieve the optimal scenario with minimal moment release, as the other cycle-related factors (e.g., injected volume and operation duration) should also be tailored to balance the energy budget. Cyclic fluid injection could be further improved with the considerations of special needs in stimulation stages and dynamic responses of faulted reservoirs, in terms of determination of dominating fault types, modulation of hydro-fracturing and hydro-shearing processes, assessment of aseismic deformation, and comprehensive response to monitoring feedbacks.

Acknowledgments

W. Wu gratefully acknowledges the support of Start-up Grant from Nanyang Technological University, Singapore. A. Zang is grateful for the funding received from the European Commission Horizon 2020 research and innovation program under grant agreement No. 691728 (DESTRESS).

References

1. Ellsworth WL. Injection-Induced earthquakes. *Science.* 2013;341(6142):1225942.
2. Majer EL, Baria R, Stark M, Oates S, Bommer J, Smith B, Asanuma H. Induced seismicity associated with Enhanced Geothermal Systems. *Geothermics.* 2007;36(3):185-222.
3. Rathnaweera TD, Wu W, Ji Y, Gamage RP. Understanding injection-induced seismicity in enhanced geothermal systems: From the coupled thermo-hydro-mechanical-chemical process to anthropogenic earthquake prediction. *Earth-Sci Rev.* 2020;205:103182.

4. Wu W, Reece JS, Gensterblum Y, Zoback MD. Permeability evolution of slowly slipping faults in shale reservoirs. *Geophys Res Lett.* 2017;44(22):11368-11375.
5. Ye Z, Ghassemi A. Injection-induced shear slip and permeability enhancement in granite fractures. *J Geophys Res Solid Earth.* 2018;23(10):9009-9032.
6. Guimaraes LN, Gomes IF, Valadares J. Influence of mechanical constitutive model on the coupled hydro geomechanical analysis of fault reactivation. SPE Reservoir Simulation Symposium. Taxes; 2009.
7. Eyre TS, Eaton DW, Garagash DI, Zecevic M, Venieri M, Weir R, Lawton DC. The role of aseismic slip in hydraulic fracturing–induced seismicity. *Sci Adv.* 2019;5(8):eaav7172.
8. Galis M, Ampuero JP, Mai PM, Cappa F. Induced seismicity provides insight into why earthquake ruptures stop. *Sci Adv.* 2017;3(12):eaap7528.
9. Ellsworth WL, Giardini D, Townend J, Ge S, Shimamoto T. Triggering of the Pohang, Korea, earthquake (M_w 5.5) by enhanced geothermal system stimulation. *Seismol Res Lett.* 2019;90(5):1844-1858.
10. Bommer JJ, Oates S, Cepeda JM, Lindholm C, Bird J, Torres R, Marroquin G, Rivas J. Control of hazard due to seismicity induced by a hot fractured rock geothermal project. *Eng Geol.* 2006;83(4):287-306.
11. Kwiatek G, Saarno T, Ader T, Bluemle F, Bohnhoff M, Chendorain M, Dresen G, Heikkinen P, Kukkonen I, Leary P, Leonhardt M. Controlling fluid-induced seismicity during a 6.1-km-deep geothermal stimulation in Finland. *Sci Adv.* 2019;5(5):eaav7224.
12. Surguchev L, Kounlin A, Melberg O, Rolfsvag TA, Menard WP. Cyclic water injection: improved oil recovery at zero cost. *Petrol Geosci.* 2002;8(1):89-95.

13. Velcin H, Dautriat J, Sarout J, Esteban L, Godel B. Experimental reactivation of shear-fractured Berea and Boise sandstones by brine or liquid CO_2 injection at depth. *J Geophys Res Solid Earth*. 2020;125(2),e2019JB018281.
14. Rutqvist J, Birkholzer J, Cappa F, Tsang CF. Estimating maximum sustainable injection pressure during geological sequestration of CO_2 using coupled fluid flow and geomechanical fault- slip analysis. Energy Convers Manag. 2007;48(6),1798–1807.
15. Zang A, Yoon JS, Stephansson O, Heidbach O. Fatigue hydraulic fracturing by cyclic reservoir treatment enhances permeability and reduces induced seismicity. *Geophys J Int.* 2013;195(2):1282-1287.
16. Zang A, Zimmermann G, Hofmann H, Stephansson O, Min KB, Kim KY. How to reduce fluid-injection-induced seismicity. *Rock Mech Rock Eng.* 2019;52(2):475-493.
17. Kwiatek G, Martínez-Garzón P, Plenkers K, Leonhardt M, Zang A, von Specht S, Dresen G, Bohnhoff M. Insights into complex subdecimeter fracturing processes occurring during a water injection experiment at depth in Äspö Hard Rock Laboratory, Sweden. *J Geophys Res Solid Earth.* 2018;123(8):6616-6635.
18. Zang A, Stephansson O, Stenberg L, Plenkers K, Specht S, Milkereit C, Schill E, Kwiatek G, Dresen G, Zimmermann G, Dahm T, Weber M. Hydraulic fracture monitoring in hard rock at 410 m depth with an advanced fluid-injection protocol and extensive sensor array. *Geophys J Int.* 2017;208(2):790-813.
19. Niemz P, Cesca S, Heimann S, Grigoli F, von Specht S, Hammer C, Zang A, Dahm T. Full-waveform-based characterization of acoustic emission activity in a mine-scale experiment: a comparison of conventional and advanced hydraulic fracturing schemes. *Geophys J Int.* 2020;222(1):189-206.

20. Hofmann H, Zimmermann G, Zang A, Min KB. Cyclic soft stimulation (CSS): a new fluid injection protocol and traffic light system to mitigate seismic risks of hydraulic stimulation treatments. *Geothermal Energy*. 2018;6(1):27.

21. Hofmann H, Zimmermann G, Farkas M, Huenges E, Zang A, Leonhardt M, Kwiatek G, Martinez-Garzon P, Bohnhoff M, Min KB, Fokker P, Westaway R, Bethmann F, Meier P, Yoon KS, Choi JW, Lee TJ, Kim KY. First field application of cyclic soft stimulation at the Pohang Enhanced Geothermal System site in Korea. *Geophys J Int.* 2019;217(2):926-949.

22. Grigoli F, Cesca S, Rinaldi AP, Manconi A, Lopez-Comino JA, Clinton JF, Westaway R, Cauzzi C, Dahm T, Wiemer S. The November 2017 M_w 5.5 Pohang earthquake: A possible case of induced seismicity in South Korea. *Science*. 2018;360(6392):1003-1006.

23. Yoon JS, Zang A, Stephansson O. Numerical investigation on optimized stimulation of intact and naturally fractured deep geothermal reservoirs using hydro-mechanical coupled discrete particles joints model. *Geothermics.* 2014;52:165-184.

24. Yoon JS, Zimmermann G, Zang A. Discrete element modeling of cyclic rate fluid injection at multiple locations in naturally fractured reservoirs. *Int J Rock Mech Min Sci.* 2015;74:15-23.

25. Ji Y, Wanniarachchi WAM, Wu W. Effect of fluid pressure heterogeneity on injection-induced fracture activation. *Comput Geotech.* 2020;123:103589.

26. Rutter E, Hackston A. On the effective stress law for rock-on-rock frictional sliding, and fault slip triggered by means of fluid injection. *Philos Trans A Math Phys Eng Sci.* 2017;375(2103):20160001.

27. Scuderi MM, Collettini C, Marone C. Frictional stability and earthquake triggering during fluid pressure stimulation of an experimental fault. *Earth Planet Sci Lett.* 2017;477:84-96.

28. Cappa F, Guglielmi Y, Nussbaum C, Birkholzer J. On the relationship between fault permeability increases, induced stress perturbation and the growth of aseismic slip during fluid injection. *Geophys Res Lett.* 2018;45(20):11012-11020.
29. Garagash DI, Germanovich LN. Nucleation and arrest of dynamic slip on a pressurized fault. *J Geophys Res Solid Earth.* 2012;117(B10).
30. Noël C, Passelègue FX, Giorgetti C, Violay M. Fault reactivation during fluid pressure oscillations: transition from stable to unstable slip. *J Geophys Res Solid Earth.* 2019;124:10940–10953.
31. Ji Y, Zhuang L, Wu W, Hofmann H, Zang A, Zimmermann G. Cyclic water injection potentially mitigates seismic risks by promoting slow and stable slip of a natural fracture in granite. *Rock Mech Rock Eng.* 2021; doi.: 10.1007/s00603-021-02438-7.
32. Wang L, Kwiatek G, Rybacki E, Bonnelye A, Bohnhoff M, Dresen G. Laboratory study on fluid- induced fault slip behavior: The role of fluid pressurization rate. *Geophys Res Lett.* 2020;47:e2019GL086627.
33. Ji Y, Wu W, Zhao Z. Unloading-induced rock fracture activation and maximum seismic moment prediction. *Eng Geol.* 2019;262:105352.
34. Ji Y, Wu W. Injection-driven fracture instability in granite: Mechanism and implications. *Tectonophysics.* 2020;791:228572.
35. Wong TF. On the normal stress dependence of the shear fracture energy. *Earthquake Source Mechanics.* 1986;37:1-11.
36. Rice JR. Constitutive relations for fault slip and earthquake instabilities. *Instabilities in Continuous Media.* 1983:443-475.

37. Marone C. The effect of loading rate on static friction and the rate of fault healing during the earthquake cycle. *Nature*. 1998;391(6662):69-72.

38. Shreedharan S, Bolton DC, Rivière J, Marone C. Preseismic fault creep and elastic wave amplitude precursors scale with lab earthquake magnitude for the continuum of tectonic failure modes. *Geophys Res Lett.* 2020;47(8):e2020GL086986.

39. Jia Y, Wu W, Kong XZ. Injection-induced slip heterogeneity on faults in shale reservoirs. *Int J Rock Mech Min Sci.* 2020;131: 104363.

40. Passelègue FX, Brantut N, Mitchell TM. Fault reactivation by fluid injection: Controls from stress state and injection rate. *Geophys Res Lett.* 2018;45(23):12837– 12846.

41. Dieterich JH, Kilgore BD. Direct observation of frictional contacts: New insights for state-dependent properties. *Pure Appl Geophys.* 1994;143(1):283-302.

42. Kilgore B, Beeler N, Lozos J, Oglesby D. Rock friction under variable normal stress. *J Geophys Res Solid Earth.* 2017;122:7042-7075.

43. Shreedharan S, Rivière J, Bhattacharya P, Marone C. Frictional state evolution during normal stress perturbations probed with ultrasonic waves. *J Geophys Res Solid Earth.* 2019;124:5469-5491.

44. McGarr A. Maximum magnitude earthquakes induced by fluid injection. *J Geophys Res Solid Earth.* 2014;119(2):1008-1019.

45. McGarr A, Barbour AJ. Injection- induced moment release can also be aseismic. *Geophys Res Lett.* 2018;45:5344-5351.

46. Landau L, Lifshitz E, Sykes J, Reid W, Dill EH. Theory of elasticity: Vol. 7 of course of theoretical physics. *Physics Today*. 1960;13:44.

47. Acosta M, Passelegue FX, Schubnel A, Violay M. Dynamic weakening during earthquakes controlled by fluid thermodynamics. *Nat Commun.* 2018;9(1):3074.

48. Passelègue FX, Almakari M, Dublanchet P, Barras F, Fortin J, Violay M. Initial effective stress controls the nature of earthquakes. *Nat Commun.* 2020;11(1):5132.

49. Aki K. Generation and propagation of G waves from the Niigata earthquake of June 16, 1964. Part 1. A statistical analysis. *Bulletin of the Earthquake Research Institute.* 1966;44(1):23-72.

50. McLaskey GC, Yamashita F. Slow and fast ruptures on a laboratory fault controlled by loading characteristics. *J Geophys Res Solid Earth.* 2017;122(5):3719-3738.

51. Scanlon BR, Weingarten MB, Murray KE, Reedy RC. Managing basin- scale fluid budgets to reduce injection- induced seismicity from the recent US shale oil revolution. *Seismol Res Lett.* 2019;90(1):171-182.

52. Im K, Elsworth D, Marone C, Leeman J. The impact of frictional healing on stick-slip recurrence interval and stress drop: Implications for earthquake scaling. *J Geophys Res Solid Earth.* 2017;122(12):10102-10117.

53. Bentz S, Kwiatek G, Martínez- Garzón P, Bohnhoff M, Dresen G. Seismic moment evolution during hydraulic stimulations. *Geophys Res Lett.* 2020;47(5): e2019GL086185.

54. De Barros L, Cappa F, Guglielmi Y, Duboeuf L, Grasso JR. Energy of injection-induced seismicity predicted from in-situ experiments. *Sci Rep.* 2019;9(1):4999.

55. Gómez Alba S, Vargas CA, Zang A. Evidencing the relationship between injected volume of water and maximum expected magnitude during the Puerto Gaitán (Colombia) earthquake sequence from 2013 to 2015. *Geophys J Int.* 2020;220(1):335-344.

56. Goodfellow SD, Nasseri MHB, Maxwell SC, Young RP. Hydraulic fracture energy budget: Insights from the laboratory. *Geophys Res Lett.* 2015;42(9):3179-3187.

57. Kanamori H. Quantification of earthquakes. *Nature.* 1978;271(5644):411-414.

58. Hanks TC, Kanamori H. A moment magnitude scale. *J Geophys Res Solid Earth.* 1979;84(B5):2348-2350.

59. Maxwell S. Unintentional seismicity induced by hydraulic fracturing. *CSEG Rec.* 2013;38(8):40-49.

60. Jalali M, Gischig V, Doetsch J, Näf R, Krietsch H, Klepikova M, Amann F, Giardini D. Transmissivity changes and microseismicity induced by small-scale hydraulic fracturing tests in crystalline rock. *Geophys Res Lett.* 2018;45(5):2265-2273.

61. Amann F, Gischig V, Evans K, Doetsch J, Jalali R, Valley B, Krietsch H, Dutler N, Villiger L, Brixel B, Klepikova M, Kittila A, Madonna C, Wiemer S, Saar MO, Loew S, Driesner T, Maurer H, Maurer H, Giardini D. The seismo-hydromechanical behavior during deep geothermal reservoir stimulations: open questions tackled in a decameter-scale in situ stimulation experiment. *Solid Earth.* 2018;9(1):115-137.

62. Zhuang L, Kim KY, Jung SG, Diaz M, Min KB, Zang A, Stephansson O, Zimmermann G, Yoon JS, Hofmann H. Cyclic hydraulic fracturing of pocheon granite cores and its impact on breakdown pressure, acoustic emission amplitudes and injectivity. *Int J Rock Mech Min Sci.* 2019;122:104065.

63. Patel SM, Sondergeld CH, Rai CS. Laboratory studies of hydraulic fracturing by cyclic injection. *Int J Rock Mech Min Sci.* 2017;95:8-15.

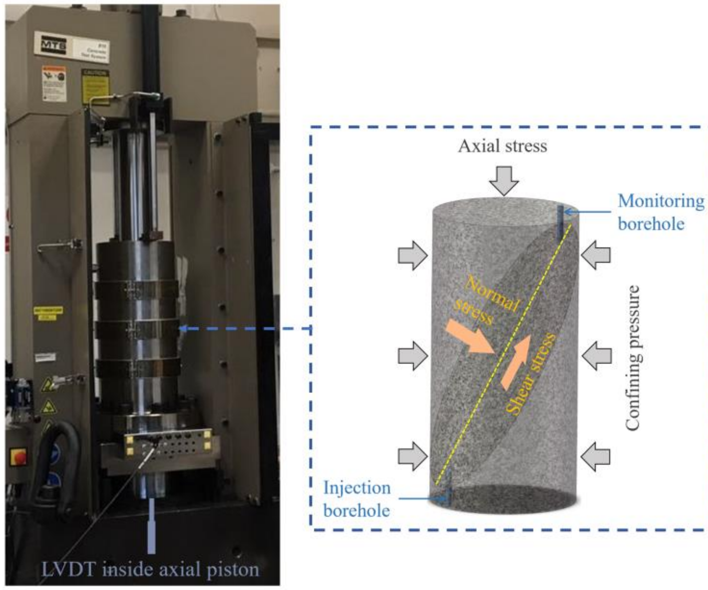

(a)

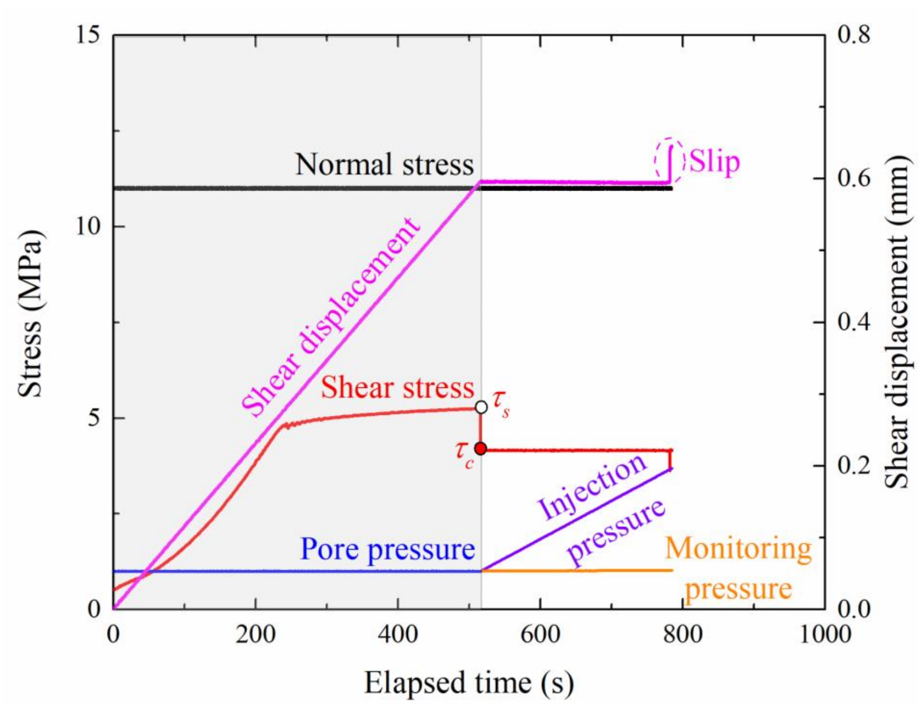

(b)

Fig. 1. (a) Fluid injection test configuration, and (b) experimental procedure: the shear strength (τ_s) of the fault is first obtained by increasing shear displacement at a rate of 1 μm/s (gray background area), and the critical shear stress (τ_c) is then maintained as 80% of the shear strength during the subsequent fluid injection test.

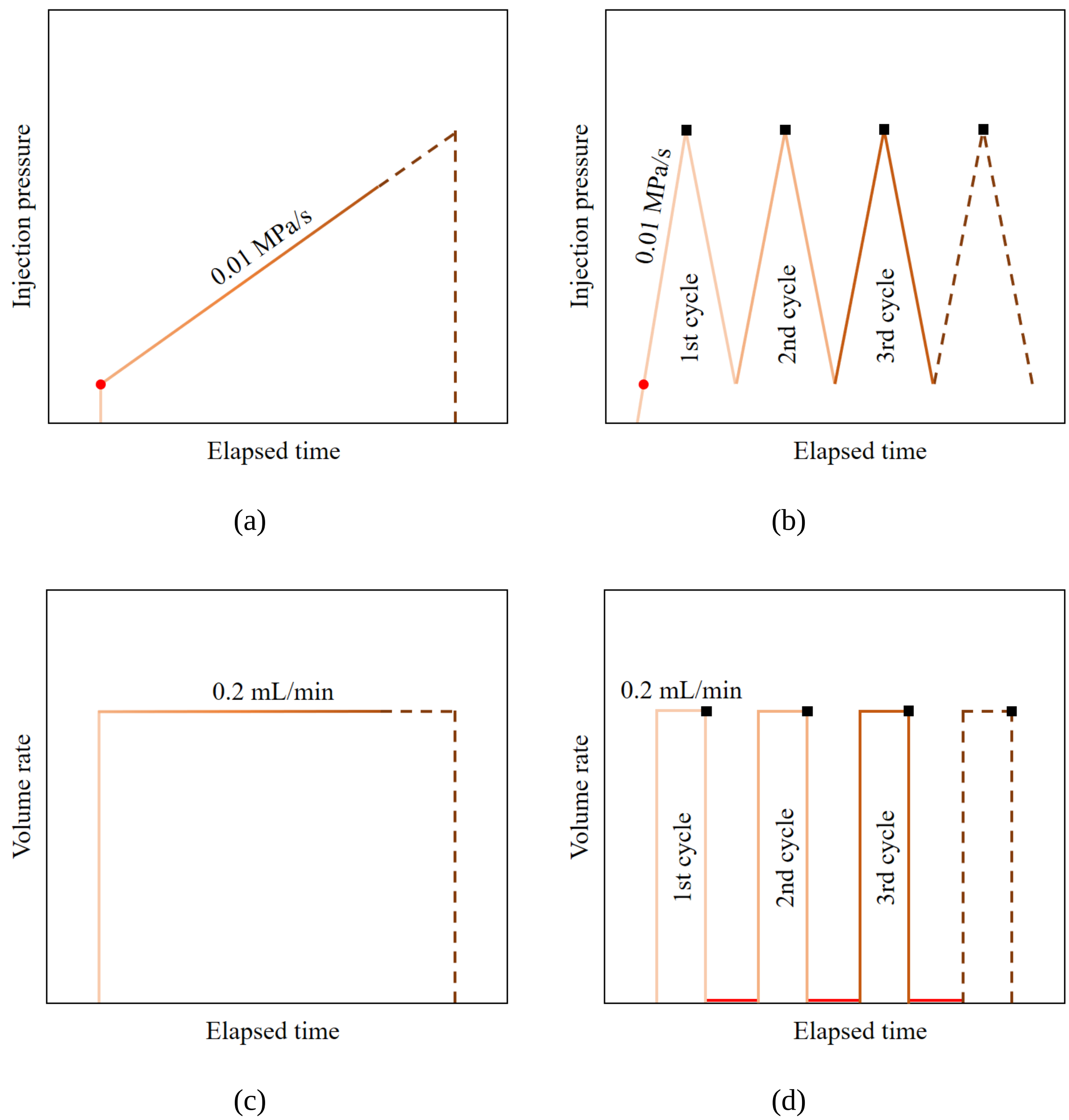

Fig. 2. Illustration of fluid injection strategies during (a) pressure-controlled monotonic injection, (b) pressure-controlled cyclic injection, (c) volume-controlled monotonic injection, and (d) volume-controlled cyclic injection. Red circle and black square denote initial and critical injection pressures, respectively. Red line indicates the duration of injection suspension (300 s).

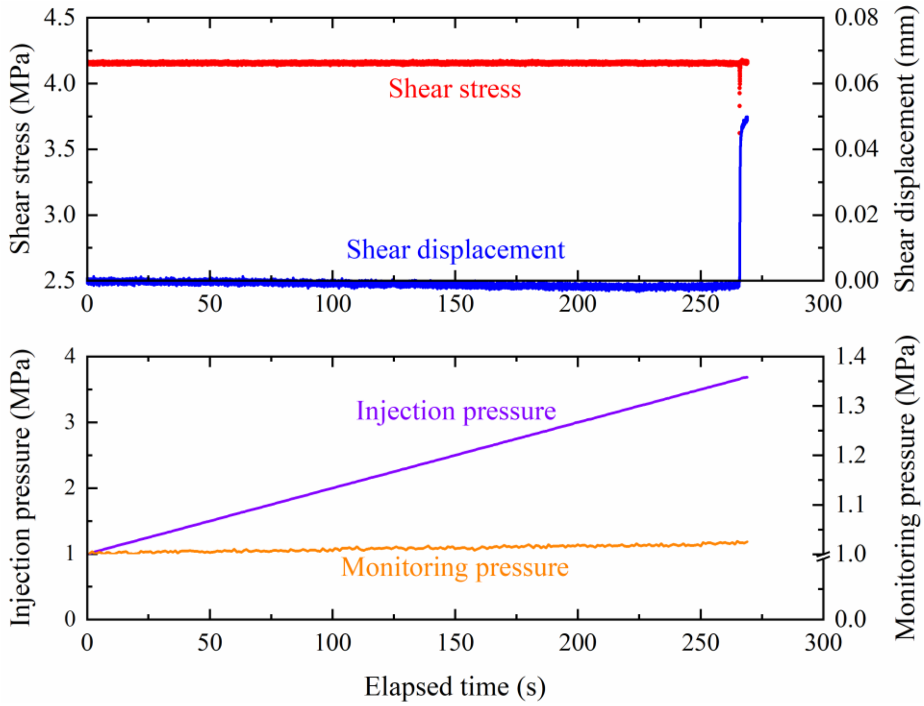
Shear stress (MPa)
Shear displacement (mm)
Shear stress
Shear displacement
Injection pressure (MPa)
Monitoring pressure (MPa)
Injection pressure
Monitoring pressure
Elapsed time (s)

(a)

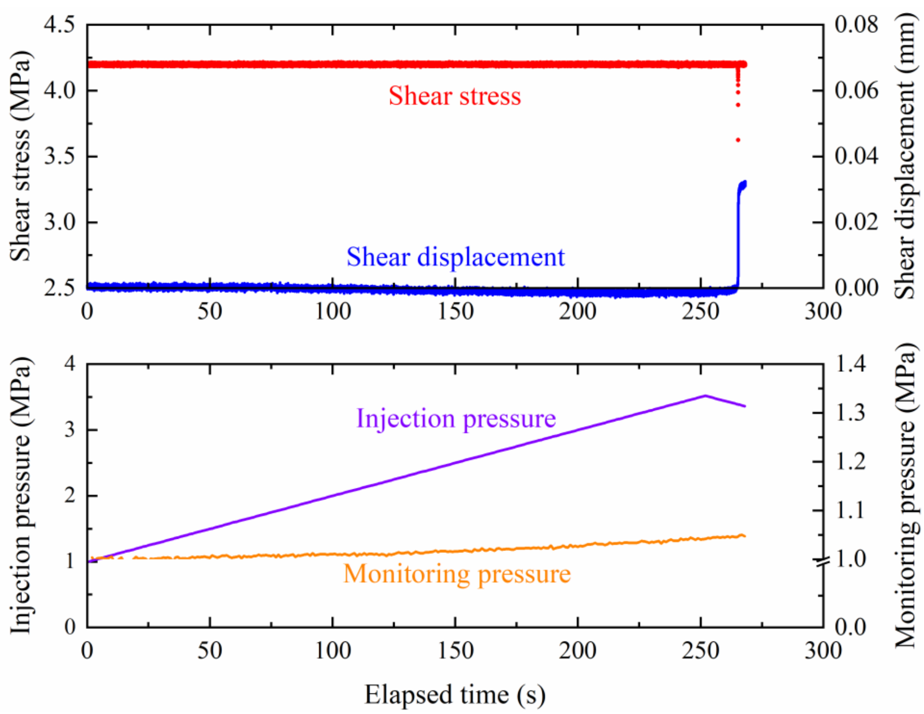
Shear stress (MPa)
Shear displacement (mm)
Shear stress
Shear displacement
Injection pressure (MPa)
Monitoring pressure (MPa)
Injection pressure
Monitoring pressure
Elapsed time (s)

(b)

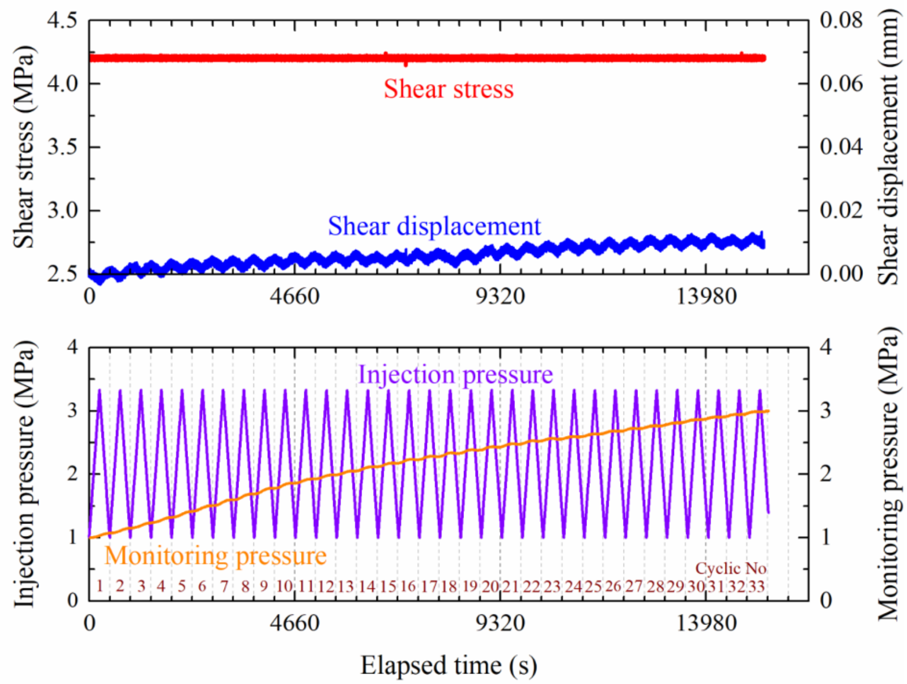

(c)

Fig. 3. Evolution of shear stress, shear displacement as well as injection and monitoring pressures during (a) pressure-controlled monotonic injection, (b) pressure-controlled cyclic injection with fault slip, and (c) pressure-controlled cyclic injection with no slip under 11 MPa normal stress.

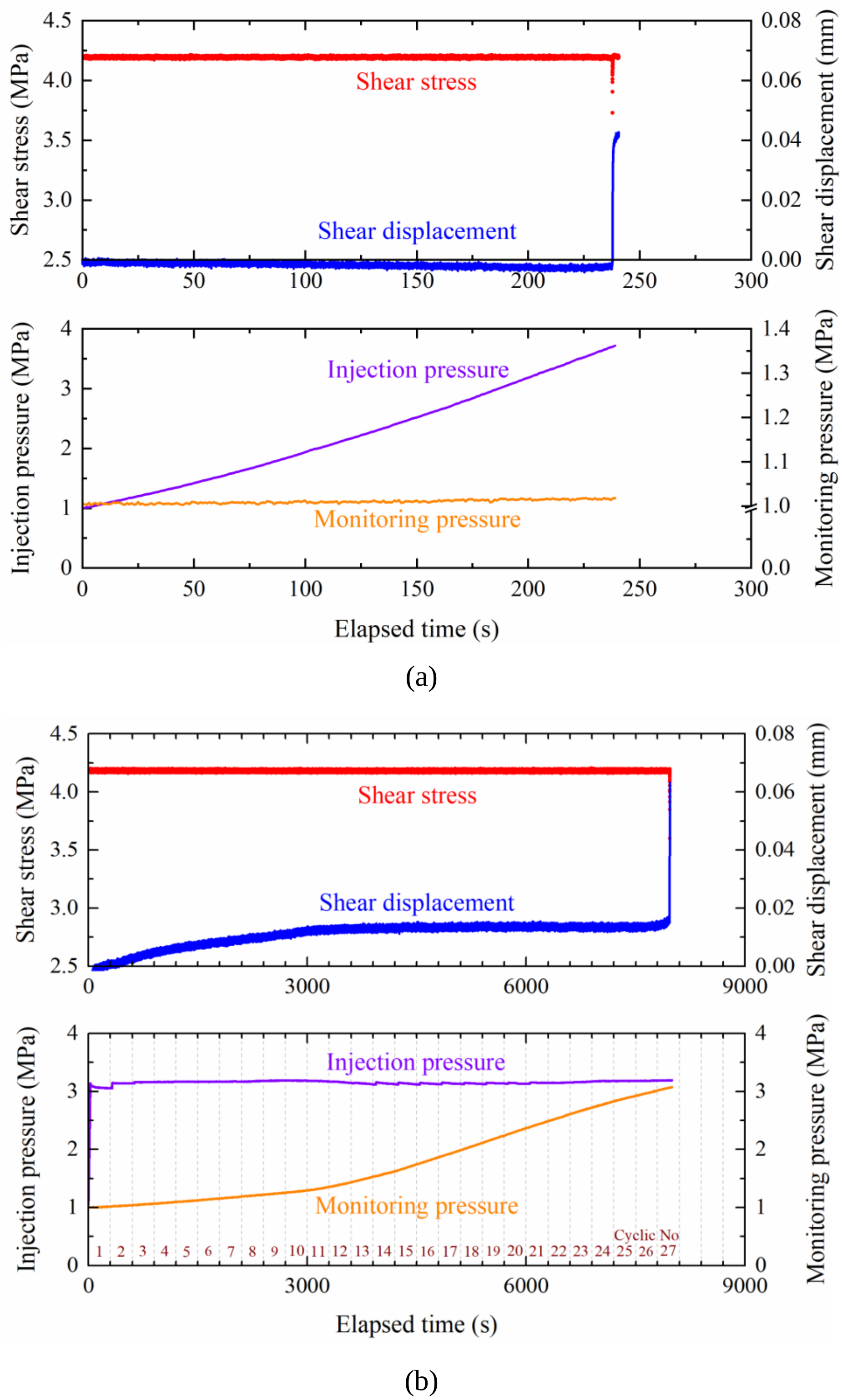

Fig. 4. Evolution of shear stress, shear displacement, as well as injection and monitoring pressures during (a) volume-controlled monotonic injection and (b) volume-controlled cyclic injection under 11 MPa normal stress.

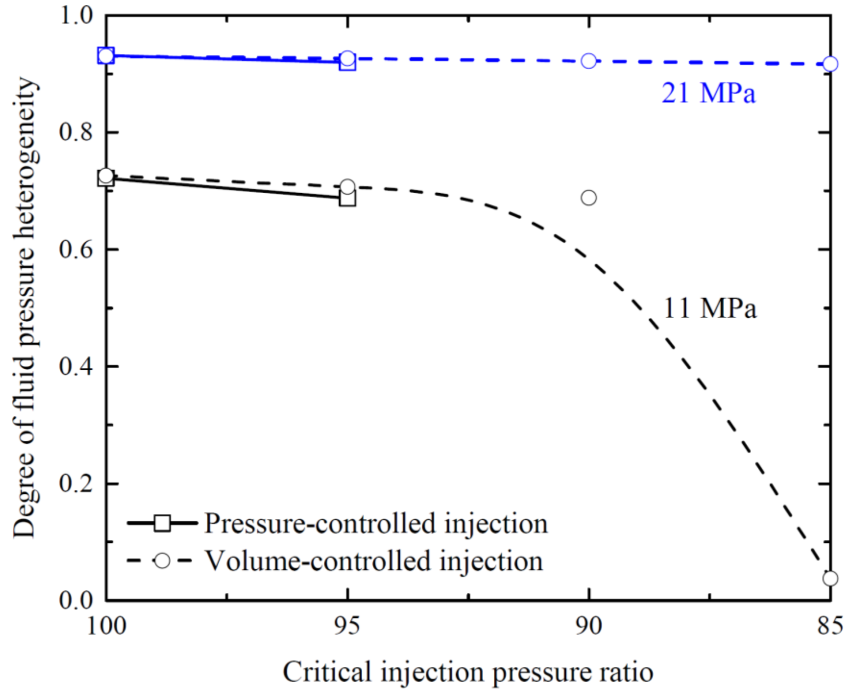

Fig. 5. Degree of fluid pressure heterogeneity reduces with decreasing critical injection pressure ratio in the cases of pressure-control and volume-control fluid injection under 11 MPa (black lines) and 21 MPa (blue lines) normal stresses, respectively. Values 0 and 1 denote the uniform fluid pressure distribution on the fault and non-uniform fluid pressure distribution with fluid pressure only accumulating around the injection borehole, respectively.

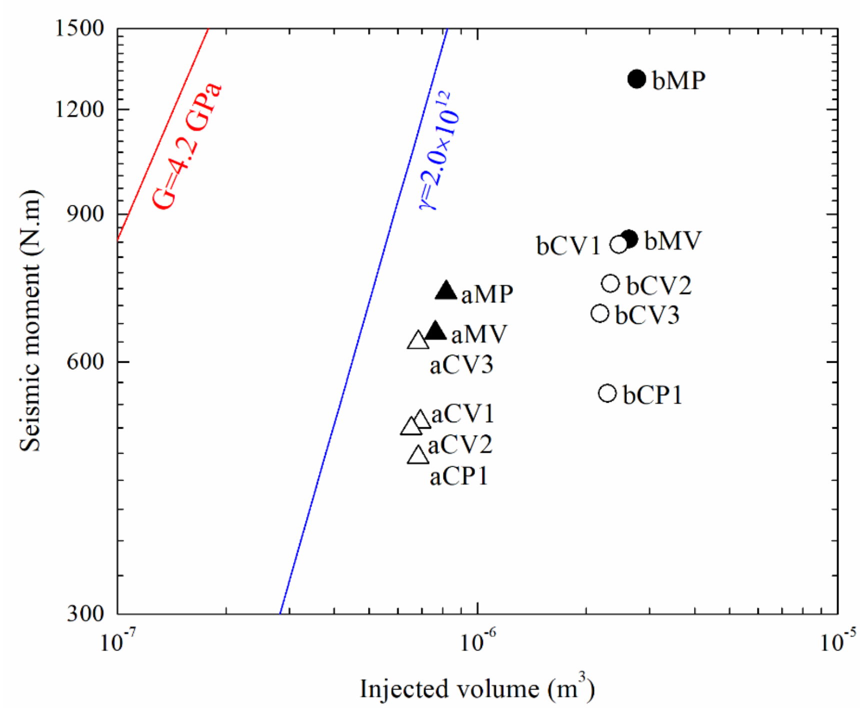

Fig. 6. Seismic moment release as a function of injected volume. Red and blue lines denote the models suggested by McGarr[38] with a modulus of rigidity (G) of 4.2 GPa and by Galis et al.[7] with a reservoir parameter (γ) of 2×10^{12}, respectively. Monotonic and cyclic fluid injection tests are marked by solid and open points, respectively. Here a and b indicate the fluid injection tests under 11 and 21 MPa normal stresses, respectively.

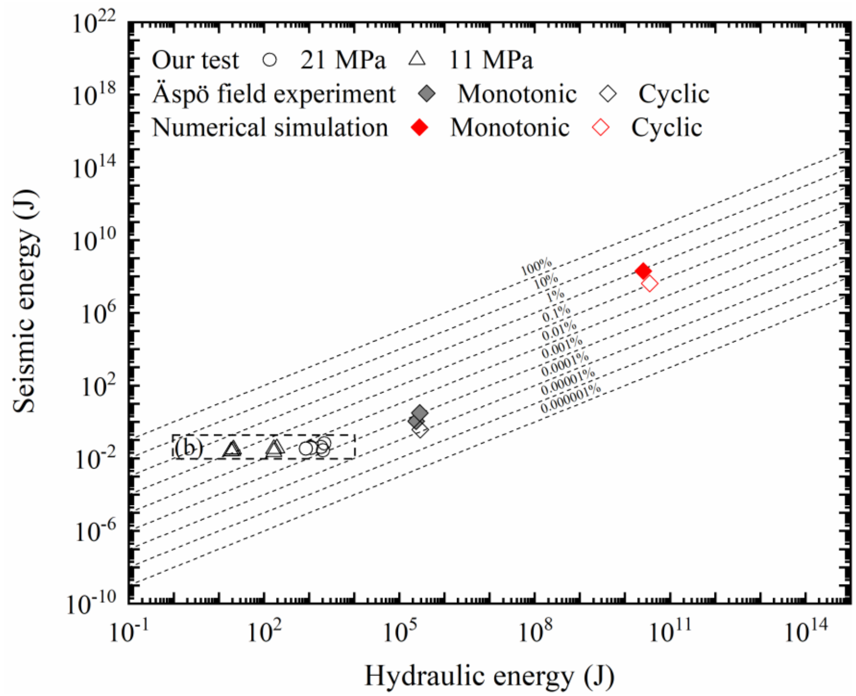

(a)

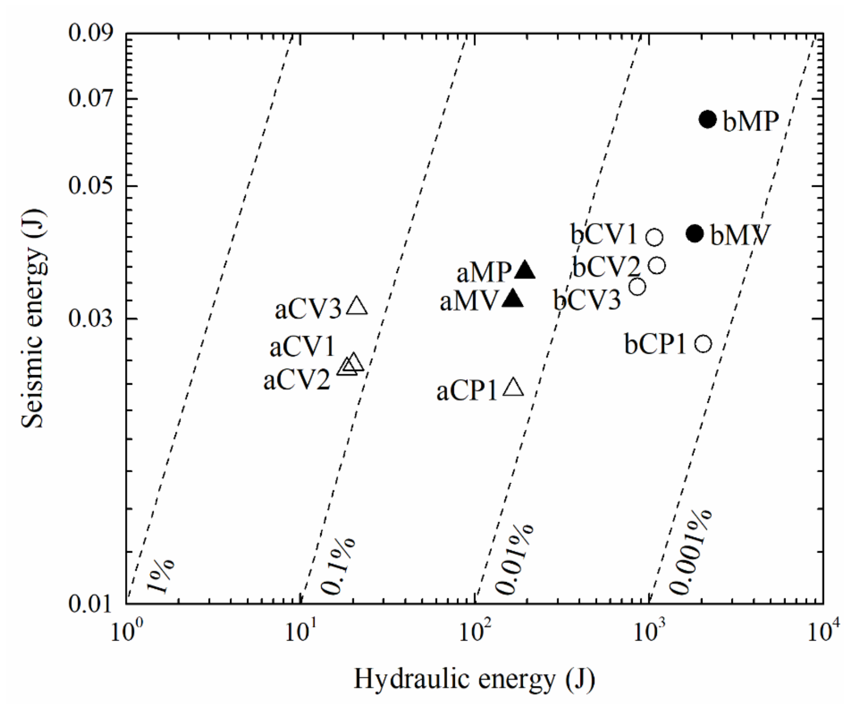

(b)

Fig. 7. (a) Seismic energy as a function of hydraulic energy. The data of Äspö field injection experiments and the corresponding numerical simulations are obtained from Kwiatek et al.[13] and Zang et al.[11,14] Black dashed lines represent the seismic injection efficiency in percentage. (b) Zoomed-in view on our data. Monotonic and cyclic fluid injection tests are denoted by solid and

open points, respectively. Here a and b indicate the fluid injection tests under 11 and 21 MPa normal stresses, respectively.

Table 1 Summary of experimental conditions and results. Here a and b indicate the fluid injection tests under 11 and 21 MPa normal stresses, respectively; M and C mean the monotonic and cyclic injection tests, respectively; P and V are the pressure-controlled and volume-controlled injection tests, respectively; $P_{f,inj,aMP}$, $P_{f,inj,aMV}$, $P_{f,inj,bMP}$ and $P_{f,inj,bMV}$ denote the injection pressures at fault failure in tests aMP, aMV, bMP and bMV, respectively.

Test	Injection rate	Critical injection pressure ratio	Cycle numbers until failure	Critical injection pressure (MPa)	Monitoring pressure at failure (kPa)	Injected volume (mm^3)	Shear stress drop (MPa)	Slip displacement (μm)	Dynamic friction coefficient
aMP	0.01 MPa/s	$P_{f,inj,aMP}$	-	3.68	1027.6	817.33	0.53	44.01	0.419
aCP1	0.01 & -0.01 MPa/s	95%$P_{f,inj,aMP}$	1	3.36	1050.1	684.29	0.57	28.00	0.412
aCP2	0.01 & -0.01 MPa/s	90%$P_{f,inj,aMP}$	33	3.33	3000.0	674.57	-	-	-
aMV	0.2 mL/min	$P_{f,inj,aMV}$	-	3.72	1018.4	763.02	0.47	39.40	0.432
aCV1	0.2 & 0 mL/min	95% $P_{f,inj,aMV}$	1	3.43	1003.9	692.43	0.42	30.85	0.427
aCV2	0.2 & 0 mL/min	90% $P_{f,inj,aMV}$	1	3.23	1008.7	653.57	0.37	30.28	0.429
aCV3	0.2 & 0 mL/min	85% $P_{f,inj,aMV}$	27	3.19	3073.0	684.29	0.58	38.35	0.457
bMP	0.01 MPa/s	$P_{f,inj,bMP}$	-	14.67	1002.5	2766.80	0.71	79.08	0.556
bCP	0.01 & -0.01 MPa/s	95%($P_{f,inj,bMP}$)	1	12.65	1019.7	2295.26	0.66	33.33	0.513
bMV	0.2 mL/min	$P_{f,inj,bMV}$	-	14.54	1011.2	2570.42	0.98	50.96	0.648
bCV1	0.2 & 0 mL/min	95% $P_{f,inj,bMV}$	1	13.77	1011.5	2467.56	1.24	50.18	0.521
bCV2	0.2 & 0 mL/min	90% $P_{f,inj,bMV}$	1	12.99	1017.2	2336.55	0.87	45.08	0.535
bCV3	0.2 &0 mL/min	85% $P_{f,inj,bMV}$	1	12.25	1021.1	2188.17	1.04	41.53	0.511